Hydrol. Earth Syst. Sci. Discuss., https://doi.org/10.5194/hess-2017-625
Manuscript under review for journal Hydrol. Earth Syst. Sci.
Discussion started: 1 November 2017

Hydrology and Earth System Sciences
Discussions

Bathymetry observations of inland water bodies using a tethered single-beam sonar controlled by an Unmanned Aerial Vehicle

Filippo Bandini[1], Daniel Olesen[2], Jakob Jakobsen[2], Cecile Marie Margaretha Kittel[1], Sheng Wang[1], Monica Garcia[1], Peter Bauer-Gottwein[1].

[1]Department of Environmental Engineering, Technical University of Denmark, Kgs. Lyngby, Denmark.
[2]National Space Institute, Technical University of Denmark, Kgs. Lyngby, 2800, Denmark.

Correspondence to: Filippo Bandini (fban@env.dtu.dk)

Abstract. High-quality bathymetric maps of inland water bodies are a common requirement for hydraulic engineering and hydrological science applications. Remote sensing methods, e.g. space-borne and airborne multispectral or LIDAR, have been developed to estimate water depth, but are ineffective for most inland water bodies, because of water turbidity and attenuation of electromagnetic radiation in water. Surveys conducted with boats equipped with sonars can retrieve accurate water depths, but are expensive, time-consuming, and are unsuitable for non-navigable water bodies.

We develop and assess a novel approach to retrieve accurate and high resolution bathymetry maps. We measured accurate water depths using a tethered floating sonar controlled by an Unmanned Aerial Vehicle (UAV) in a Danish lake and in a few river cross sections. The developed technique combines the advantages of remote sensing techniques with the potential of bathymetric sonars. UAV surveys can be conducted also in non-navigable, inaccessible, or remote water bodies. The tethered sonar can measure bathymetry with an accuracy of ca. 2.1% of the actual depth for observations up to 35 m, without being significantly affected by water turbidity, bedform or bed material.

1. Introduction

Accurate topography data of the riverbed and floodplain areas are crucial elements in hydrodynamic models. Detailed bathymetry maps of inland water bodies are essential for simulating flow dynamics and forecasting flood hazard (Amir et al., 2014; Conner and Tonina, 2014; Gichamo et al., 2012; Schäppi et al., 2010), predicting sediment transport and streambed morphological evolution (Manley and Singer, 2008; Nitsche et al., 2007; Rovira et al., 2005; Snellen et al., 2011), and monitoring instream habitats (Brown and Blondel, 2009; Powers et al., 2015; Strayer et al., 2006; Walker and Alford, 2016). While floodplain areas can be directly monitored from aerial surveys, riverbed topography is not directly observable from airborne or space-borne methods (Alsdorf et al., 2007). Thus, there is a widespread global deficiency in bathymetry measurements of rivers and lakes.

Within the electromagnetic spectrum, visible wavelengths have the greatest atmospheric transmittance and the smallest water attenuation (Liu et al., 2010). Therefore, remote sensing imagery from satellites such as Landsat (Liceaga-Correa and Euan-Avila, 2002), Quickbird (Lyons et al., 2011), IKONOS (Stumpf et al., 2003), Worldview-2 (Hamylton et al., 2015; Lee et al., 2011), and aircraft (Carbonneau et al., 2006; Marcus et al., 2003), has been used to monitor the bathymetry of inland water bodies. However, bathymetry can only be indirectly derived from optical imagery when water is very clear and shallow, the sediment is comparatively homogeneous, and the atmosphere is favorable (Lyzenga, 1981; Lyzenga et al., 2006). Thus,

applications are limited to gravel-bed shallow rivers, in which water depth is on the order of Secchi depth (depth at which a Secchi disk is no longer visible from the surface).

Similarly airborne LIDARs can be applied to retrieve bathymetry maps (Bailly et al., 2010; Hilldale and Raff, 2008; Legleiter, 2012), but this method is limited by water turbidity, which severely restricts the maximum depth to generally 2-3 times Secchi depth (Guenther, 2001; Guenther et al., 2000).

Because of satellite or aircraft remote sensing limitations, accurate bathymetric cross sections are generally obtained during field surveys, which are expensive and labor intensive. Some preliminary tests using pulses of a green wavelength (λ =532 nm) Terrestrial Laser Scanning (TLS) for surveying submerged areas have been performed (Smith et al., 2012; Smith and Vericat, 2014). However, TLS suffers from similar limitations as LIDAR. Furthermore, the highly oblique scan angles of TLS make refraction effects more problematic (Woodget et al., 2015) and decrease returns from the bottom while increasing returns from the water surface (Bangen et al., 2014). Therefore, field surveys are normally performed using single-beam or multi-beam sonars generally transported on manned boats or more recently on unmanned vessels (e.g. Brown et al. 2010; Ferreira et al. 2009; Giordano et al. 2015) . However, boats cannot be employed along non-navigable rivers and require sufficient water depth for navigation.

Unmanned Aerial Vehicles (UAVs) offer the advantage of enabling a rapid characterization of water bodies in areas that may be difficult to access by human operators (Tauro et al., 2015b). Bathymetry studies using UAVs are so far restricted to i) passive spectral signature-depth correlation (Flener et al., 2013; Lejot et al., 2007) or ii) DEM (Digital Elevation Model) generation through stereoscopic techniques from through-water pictures, correcting for the refractive index of water (Bagheri et al., 2015; Dietrich, 2016; Tamminga et al., 2014; Woodget et al., 2015).

The high cost, size, and weight of bathymetric LIDARs severely limit their implementation on UAVs. An exception is the novel topo-bathymetric laser profiler, Bathymetric Depth Finder BDF-1 (Mandlburger et al., 2016). This LIDAR profiler can retrieve measurements up to 1-1.5 time Secchi Depth, thus it is only suitable for gravel-bed shallow water. The system weighs ca. 5.3 kg and requires a large UAV platform, e.g. multi-copters with a weight around 25 kg.

To overcome these limitations, we assess a new operational method to estimate river bathymetry in deep and turbid rivers. This new technique consists in employing a tethered floating off-the-shelf sonar controlled by a UAV. With this technique we can combine i) the advantages of UAVs in surveying also remote, dangerous, non-navigable areas, with ii) the capability of bathymetric sonars of measuring bathymetry in deep and turbid inland water bodies.

UAV-measurements of water depth (i.e. elevation of the water surface above the bed) can enrich the set of available hydrological observations along with measurements of water level, i.e. elevation of the water surface above sea level, (Bandini et al., 2017) and surface water flow (Detert and Weitbrecht, 2015; Tauro et al., 2015a, 2016; Virili et al., 2015).

2. Materials and methods

The UAV used for this study was a multi-copter: the off-the-shelf DJI hexa-copter Spreading Wings S900 equipped with a DJI A-2 flight controller.

2.1. Sonar instrumentation

The sonar used for this study was the “Deeper Smart Sonar Pro Plus” developed by the company Deeper, UAB. It costs ≈$240 and weighs ≈100 g.

The sonar is tethered to the UAV with a physical wire connection as shown in Figure 1. For specific applications, the sonar can be lowered or raised using a remotely controlled lightweight wire winch, as shown in Figure 1. The maximum extension

Hydrol. Earth Syst. Sci. Discuss., https://doi.org/10.5194/hess-2017-625
Manuscript under review for journal Hydrol. Earth Syst. Sci.
Discussion started: 1 November 2017

of the wire was ca. 5 m. Furthermore a remotely controlled emergency hook can be installed to release the sonar in case of emergency, e.g. if the wire is caught in obstacles.

Figure 1. Deeper sonar is connected to a UAV with a wire winch.

This sonar is a single-beam echo-sounder with two frequencies: 290 kHz and 90 kHz, with 15° and 55° beam angles respectively. The 90 kHz frequency was specifically developed to identify fish with a large scanning angle, while the narrow field of view of the 290 KHz frequency gives the highest bathymetric accuracy. For this reason the 290 KHz frequency is used for observing bottom structure. The 15° beam divergence of the 290 kHz frequency results in a ground footprint of ca. 26 cm at 1 m water depth. The sonar is capable of measuring depths up to 80 m.

The observations retrieved by the sonar include: time, approximate geographical coordinates of the sonar, sonar depth measurements including waveform shape, size and depth of identified fish, and water temperature. Analysis of the multiple echo returns of the sonar wave is essential to identify the actual measurement of the water depth. Indeed, when a sound pulse returns from the bottom, only a very small part of the echo hits the receiving transducer. The major portion hits the water surface and is reflected back to the bottom of the water body. Then it is reflected again, and hits the receiving transducer a second time. In shallow water this double-path reflection is strong enough to generate a second echo that must be filtered out.

2.2. UAV payload

The UAV was equipped with GNSS (Global Navigation Satellite System) for retrieving accurate position, an IMU (Inertial Measurement Unit) to retrieve angular and linear motion, and a radar system to measure the range to water surface. A picture of the UAV and the tethered sonar is shown in Figure 2.

Hydrol. Earth Syst. Sci. Discuss., https://doi.org/10.5194/hess-2017-625
Manuscript under review for journal Hydrol. Earth Syst. Sci.
Discussion started: 1 November 2017

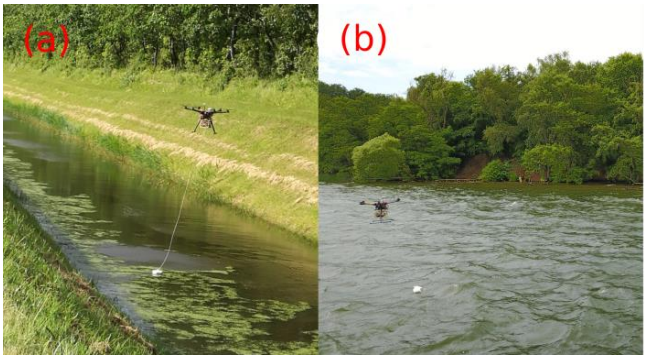

Figure 2. Pictures of the UAV and the tethered sonar. These pictures were retrieved in: (a) Marrebæk Kanal, Denmark. (b) Furesø lake, Sjælland, Denmark. In (b) the drone was flown a few hundreds of meters from the coastline and the picture was retrieved using an optical camera onboard an auxiliary UAV (DJI Mavic Pro).

The on-board GNSS system is a NovAtel receiver (OEM628 board) with an Antcom (3G0XX16A4-XT-1-4-Cert) dual frequency GPS and GLONASS flight antenna. To estimate drone position with cm accuracy, the GNSS system works in carrier phase differential GPS mode. The on-board Inertial Measurement Unit (IMU) is an Xsense MTi 10-series. The optical camera is a SONY RX-100 camera. The radar is an ARS 30X radar developed by Continental.

The radar and GNSS systems are the same instrumentation as described in Bandini et al. (2017), where the system was developed to measure water level (i.e. height of the water surface above reference geoid). Water level was measured by subtracting the range measured by the radar (range between the UAV and the water surface) from the altitude observed by the GNSS instrumentation (i.e. altitude above reference ellipsoid, convertible into altitude above geoid level).

In this research, the radar and GNSS instrumentation are used i) to retrieve water level ii) to observe the accurate position of the tethered sonar.

2.3. Computation of sonar position

The sonar has a built-in GPS receiver to identify its approximate location. However, the accuracy of this GPS is several meters (up to 30 m). The large error of this single frequency GPS receiver is related to many different factors, including that both water beneath the sonar and the drone above disturb the GPS signal. The accuracy of either GPS option is suboptimal for the generation of bathymetry maps, thus more accurate measurements of the sonar position are necessary. The drone absolute position is accurately known through the differential GNSS system described in Bandini et al. (2017). In order to estimate the relative position of the sonar with respect to the drone, the payload system measures the offset and orientation of the sonar. This concept is described in Figure 3.

Hydrol. Earth Syst. Sci. Discuss., https://doi.org/10.5194/hess-2017-625
Manuscript under review for journal Hydrol. Earth Syst. Sci.
Discussion started: 1 November 2017

Hydrology and Earth System Sciences
Discussions

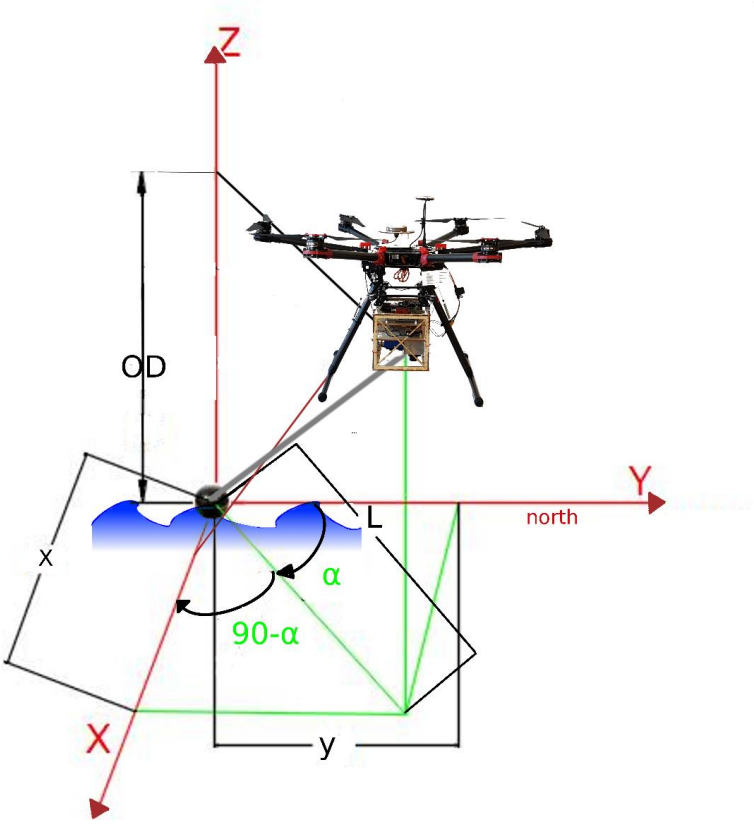

Figure 3. Sonar is the center of the reference system X, Y, Z. The horizontal displacement between the sonar and the drone is computed along the X and Y directions, the vertical displacement along the Z axis (Object Distance - OD). α is the azimuth, the angle between the Y-axis pointing north and the vector between the drone and the sonar, projected onto the horizontal plane (in green). The azimuth is measured clockwise from north (i.e. α is positive in the figure).

As shown in Figure 3 the azimuth angle is necessary to compute the sonar displacement in Cartesian geographical coordinates. Thus, the variables to compute are x and y, which represent the displacement between the sonar and the camera sensor, measured in easting and northing respectively.

The horizontal displacement between the sonar and the onboard camera is retrieved using the equations displayed in Table 1. These equations require observations from the different sensors of the drone payload: optical camera, radar, IMU, and differential GNSS system.

Pictures are taken by the optical SONY camera with focus set to infinity. Lens distortion needs to be removed, since the SONY RX-100 camera is not a metric camera. Numerous methods have been discussed in the literature to correct for lens distortion (e.g. Brown, 1971; Clarke & Fryer, 1998; Faig, 1975; Weng et al., 1992). In this research the software PTLENS was used to remove lens radial distortion as the program database already includes the specific lens parameters for the SONY RX-100 camera. Eventually image units (pixels) can be converted into metric units.

Hydrol. Earth Syst. Sci. Discuss., https://doi.org/10.5194/hess-2017-625
Manuscript under review for journal Hydrol. Earth Syst. Sci.
Discussion started: 1 November 2017

Hydrology and Earth System Sciences
Discussions

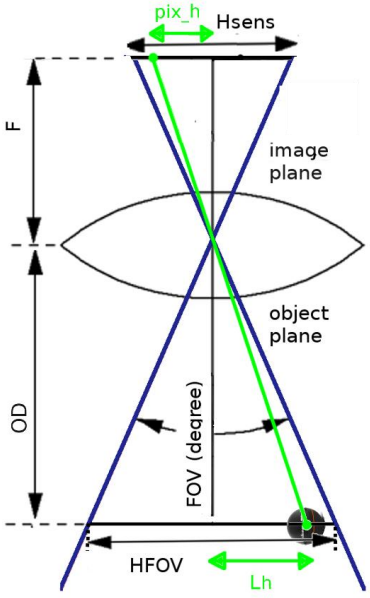

Figure 4. Relationship between FOV (field of view in degree), HFOV (height of the field of view, in metric unit), OD (object distance), F (focal length), pix_h (distance in pixels between center of the image and object in the image, along vertical axis of the image), and Lh (distance in metric units between object and center of the sensor, along vertical axis of the image). The drawing is valid under the assumption that the image distance (distance from the lens to the image plane) corresponds to the focal length.

The WFOV and HFOV (width and height of the field of view) are estimated with Eq. *(1)* from the Wsens and Hsens (sensor width and height), the focal length (F) and the OD. OD is the vertical range to the water surface, on which the sonar is floating and is measured by the radar. A representation of the image plane and object plane is given in Figure 4.

Equation *(3)* and *(4)* compute the displacement, in metric unit, between the sonar and the center of the camera sensor along the horizontal (Lw) and vertical (Lh) axis of the picture, taking as input the size field of view in metric units, the resolution in pixels of the sensor along the two axis, n_{pix_w} and n_{pix_h}, and the measured distance in pixels between the sonar and the center of the image along the horizontal and vertical image axis, pix_w and pix_h, respectively. In Figure 5 we show a picture retrieved by the camera. In the current payload setup the vertical axis of the camera is aligned with the drone nose (heading). The displacement vector, L, and the angle, φ, are computed through Eq. *(5)* and *(6)*.

The azimuth angle α of the sonar is computed through Eq. *(7)*, in which β is the drone heading (angle between the drone's nose and the direction of the true north, measured clockwise from north). The heading is measured by the onboard IMU system.

Hydrol. Earth Syst. Sci. Discuss., https://doi.org/10.5194/hess-2017-625
Manuscript under review for journal Hydrol. Earth Syst. Sci.
Discussion started: 1 November 2017

Hydrology and Earth System Sciences
Discussions
Open Access
EGU

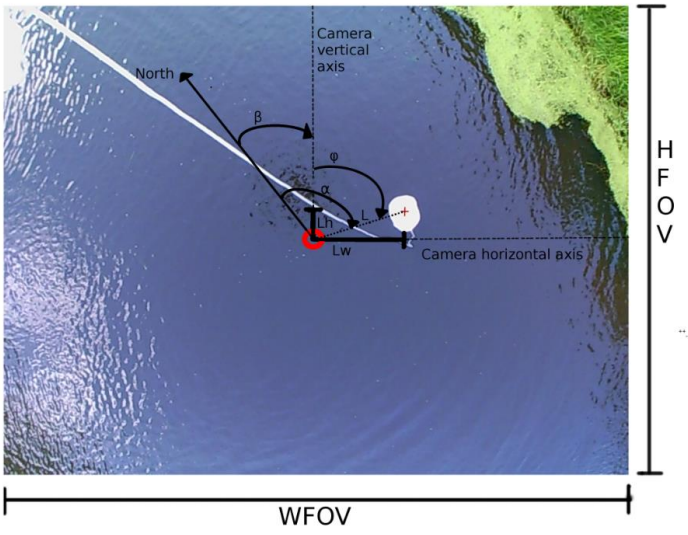

Figure 5. UAV-borne picture of the tethered sonar. The tethered sonar is located below the white polyester board floating on the water surface. The red circle indicates the center of the image, while the red cross indicates the exact position of the sonar. The North direction is retrieved by the IMU. The vertical axis of the camera coincides with the drone heading. β is the angle between the drone heading and the north. φ is the angle measured clockwise from the camera vertical axis to the vector (L), which is the vector on the horizontal plane connecting the sonar to the image center. α is the angle measured clockwise from the north direction to L. Angles and vectors highlighted in this figure are on the horizontal plane, i.e. the water surface.

Table 1. Equations to compute displacement of the sonar with respect to the onboard camera. Heading and azimuth angles are measured clockwise from north (i.e. negative angles when the direction is counterclockwise).

$$WFOV = Wsens \cdot \frac{OD}{F} \quad (1)$$

$$HFOV = Hsens \cdot \frac{OD}{F} \quad (2)$$

$$Lw = \frac{WFOV}{n_{pix\_w}} \cdot pix\_w \quad (3)$$

$$Lh = \frac{HFOV}{n_{pix\_h}} \cdot pix\_h \quad (4)$$

$$L = \sqrt{Lw^2 + Lh^2} \quad (5)$$

$$\varphi = \tan^{-1}\frac{Lw}{Lh} \quad (6)$$

$$\alpha = \beta + \varphi \quad (7)$$

$$x = \cos(90 - \alpha) \cdot L \quad (8)$$

$$y = \sin(90 - \alpha) \cdot L \qquad (9)$$

The computed variables x and y represent the geographical coordinates of the relative position of the drone with respect to the camera sensor onboard the drone. The absolute position of the drone is retrieved by the GNSS antenna installed on the top of the drone. The offset between the sensor of the camera onboard the drone and the phase center of the GNSS antenna position is constant and known a priori. This offset vector also needs to be converted to geographical coordinates for each time step taking into account the drone heading.

Using this framework, the absolute sonar position can be computed in geographical coordinates.

2.4. Case studies

First the accuracy of the sonar in measuring water depth was assessed against measurements from survey boats. Secondly, UAV surveys were conducted to evaluate the sonar accuracy in measuring depth and the accuracy in determining sonar position.

2.4.1. On boat accuracy evaluation

A bathymetric survey was conducted on a boat in Furesø lake, Denmark.

A second reference sonar, SS510 Smart™ Sensor, was employed to assess the accuracy of the Deeper sonar. According to the technical datasheet, the SS510 Smart™ Sensor weighs around 1.3 kg, has a resolution of 3 cm, 9° beam angle, a measuring range from 0.4 m to 200 m and nominal accuracy 0.25% in depth measurements at full range. Data between the two sonars were synchronized and accurate horizontal locations were acquired with a RTK GNSS rover station installed on the boat.

During this survey ground truth water depth measurements were retrieved in selected locations to validate the observations of the two sonars. Ground truth measurements were retrieved using a measuring system consisting of a heavy weight (ca. 5 kg) attached to an accurate measuring tape. This reference system is supposed to have an accuracy of ca. 10-15 cm in water depth up to 40 m.

2.4.2. UAV-borne measurements

Flights were conducted in Denmark above Furesø lake, Sjælland and above Marrebæk Kanal, Falster. The flights above Furesø demonstrate the potential of the airborne technology for taking measurements at a line–of-sight distance of a few hundred meters from the coastline.

The flight above Marrebæk Kanal demonstrates the possibility of retrieving accurate river cross sections, which can potentially be used to inform hydrodynamic river models. The accuracy of the observed river cross sections is evaluated by comparison with ground truth observations. Ground truth observations in Marrebæk Kanal were obtained by a manual operator wading into the river and taking measurements with an RTK GNSS station of i) the orthometric height of the river bottom, ii) the orthometric height of water level, and iii) the water depth, computed by subtracting the orthometric height of the bottom from the water level measurements.

Hydrol. Earth Syst. Sci. Discuss., https://doi.org/10.5194/hess-2017-625
Manuscript under review for journal Hydrol. Earth Syst. Sci.
Discussion started: 1 November 2017

3. Results

3.1. Computation of the sonar position

The accuracy of the estimation of the absolute position of the sonar in geographical coordinates depends on the accuracy of: i) the horizontal drone position, ii) the drone heading, and iii) the relative position of the sonar with respect to the drone. The accuracy of these observations is reported in Table 2.

The accuracy in measuring the relative position of the sonar depends on image analysis procedure to convert an offset from pixel into metric units. This procedure is also affected by radar accuracy in measuring the range to the target, since OD is an input to *(1)* and *(2)*. Tests were conducted in static mode using a checkerboard, placed at a known distance values in the range between 1 and 4 m, to evaluate the accuracy of measuring true distances in the image. These experiments proved an accuracy in measuring the offset between the camera and the sensor of ≈3% of its actual value. This error in converting from image units to true distance units is mainly due to i) uncorrected lens distortion and ii) approximation for equations *(1)* and *(2)* in assuming the distance between the lens and the image plane exactly equal to focal length.

Table 2. Accuracy of the different sensors which are used to measure the absolute position of the sonar in geographical coordinates

Sensor	Observation	Accuracy
IMU	β (drone heading)	3°
GNSS	Drone horizontal position	2 cm at twice the standard deviation (Bandini et al., 2017)
Radar	OD (range to water surface)	0.5% of the actual range (Bandini et al., 2017)
Camera	Lw, Lh (Offset between sonar and camera center along horizontal and vertical axis of the picture)	≈3% of the actual value

An error propagation study was performed to evaluate the overall accuracy in obtaining the absolute position of the sonar in horizontal coordinates. For detailed information, see the supplementary data. The errors in measuring β and in computing Lw and Lh have the larger impact on the overall accuracy, compared to other error sources, such as OD and drone absolute position. Since the offset between the center of the camera and the sonar, L, typically assumes values between 0 and 2 m, the overall sonar position accuracy is generally better than 20 cm. This accuracy is acceptable for most bathymetric surveys, particularly in light of the spatial resolution (15° beam divergence) of the sonar measurements.

3.2. On boat sonar accuracy

Figure 6 shows the measurements retrieved by the two sonars in the lake. The background of the maps is from Google Satellite imagery. The water level retrieved by the RTK GNSS station was 20.40 ±0.05 m above sea level during this survey. The orthometric height of the bottom can be retrieved by subtracting water depth observations from the water level.

Hydrol. Earth Syst. Sci. Discuss., https://doi.org/10.5194/hess-2017-625
Manuscript under review for journal Hydrol. Earth Syst. Sci.
Discussion started: 1 November 2017

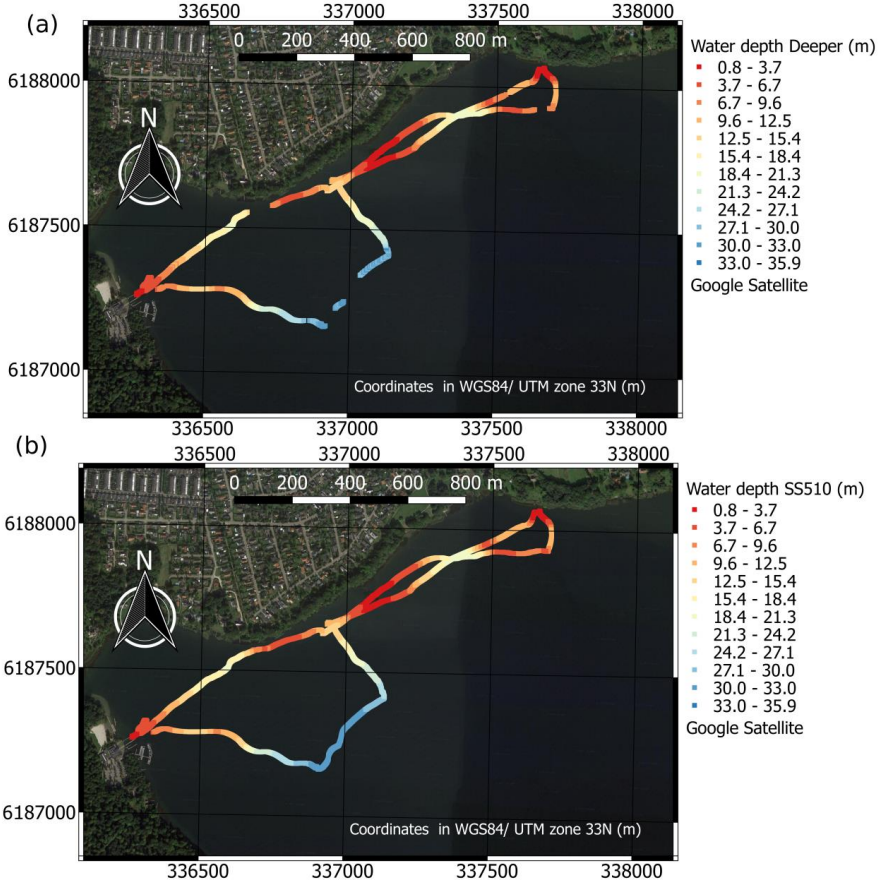

Figure 6. Water depth measurements retrieved in Furesø by the two sonars: (a) Observations with Deeper sonar; (b) observations with SS510 sonar.

The maximum water depth retrieved during the survey is ca. 35 m.

In Figure 7 we report the absolute value of the difference between the observations retrieved by the two sonars.

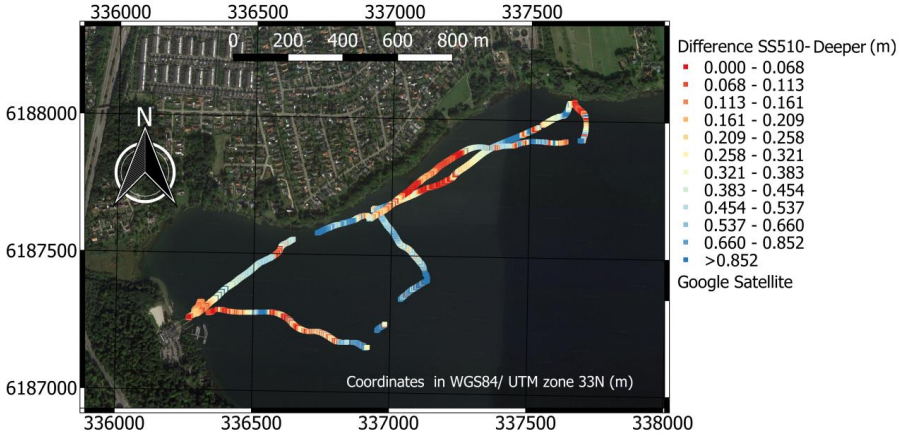

Figure 7. Absolute value of the difference between water depth measured by SS510 sonar and the Deeper sonar.

Figure 7 shows high consistency between the two sonars. However, coastal areas with dense submerged vegetation result in larger errors. While in the deepest area (ca. 30 m deep) the Deeper sonar observed multiple returns of the sound wave caused

by suspended sediments, thus the analysis of the waveform was more complicated and subject to errors. In this area the Deeper sonar is missing some water depth observations, where the waveform analysis does not show a well-defined strong returning echo.

The observations retrieved by the two sonars are compared with ground truth observations in Figure 8.

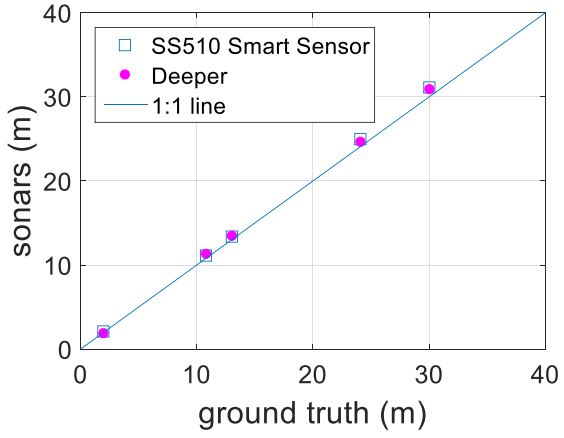

Figure 8. Relationship between measurements of two sonars and ground truth.

Regression lines could be fitted to the observations shown in Figure 8 with a R^2 of ca. 0.99. Figure 8 depicts a systematic underestimation of water depth by both sensors with a clear constant slope. This suggests that the bias can be corrected to enhance survey accuracy. In appendix A we shortly describe the physical variables (depth, salinity and temperature) affecting sonar measurements.

Table 3 shows comparative statistics between the Deeper, the SS510 sonar and the ground truth observations.

Hydrol. Earth Syst. Sci. Discuss., https://doi.org/10.5194/hess-2017-625
Manuscript under review for journal Hydrol. Earth Syst. Sci.
Discussion started: 1 November 2017

Table 3. Statistics comparing the Deeper sonar, SS510 sonar and ground truth observations.

Statistics	SS510 sonar-Deeper sonar[a]	Deeper sonar-ground truth[b]	SS510 sonar-ground truth[b]	Deeper sonar-ground truth[c]	SS510 sonar-ground truth[c]
Sample size	57528	5	5	5	5
Root mean Square Error (RMSE) [m]	0.38	0.58	0.675	0.12	0.052
Mean absolute error (MAE) [m]	0.32	0.52	0.560	0.11	0.047
Mean bias error (MBE) [m]	0.27	0.480	0.560	$5*10^{-4}$	-0.01
Relative error [%]	3.7%	3.8%	3.65%	2.1%	0.57%

[a] Statistics computed after removing outliers (above the 95% percentile and below the 5% percentile).
[b] Before bias correction
[c] After bias correction

Table 3 shows a difference of ca. 30 cm between the measurements of the two sonars, with the Deeper sonar generally underestimating water depth. This can be due to the wider scanning angle of the Deeper (15°) compared to the SS510 sonar (9°). The Deeper is more affected by steep slopes, in which the depth tends to be biased toward the shallowest point in the beam because of the larger scanning angle. The Deeper and SS510 observations can be corrected by applying a correction factor that considers the difference between sonar measurements and ground truth. The correction factors were found to be 0.97 for the Deeper and 0.96 for the SS510 sonar. The correction factor is site specific as it depends on the bed form and material, and on the water condition (temperature, salinity, and pressure). Therefore, the acquisition of a sample of ground control points is required.

3.3. UAV-borne measurements

In Figure 9 we show the observations of the UAV-borne survey above Furesø.

Hydrol. Earth Syst. Sci. Discuss., https://doi.org/10.5194/hess-2017-625
Manuscript under review for journal Hydrol. Earth Syst. Sci.
Discussion started: 1 November 2017

Hydrology and Earth System Sciences
Discussions

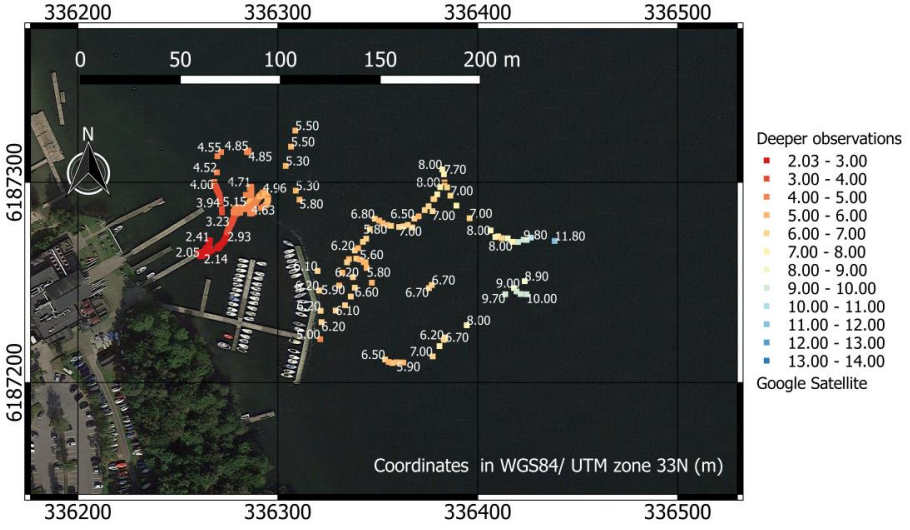

Figure 9. Airborne water depth (m) observations in Furesø.

Figure 10 depicts the UAV observations of four different cross sections of Marrebæk Kanal.

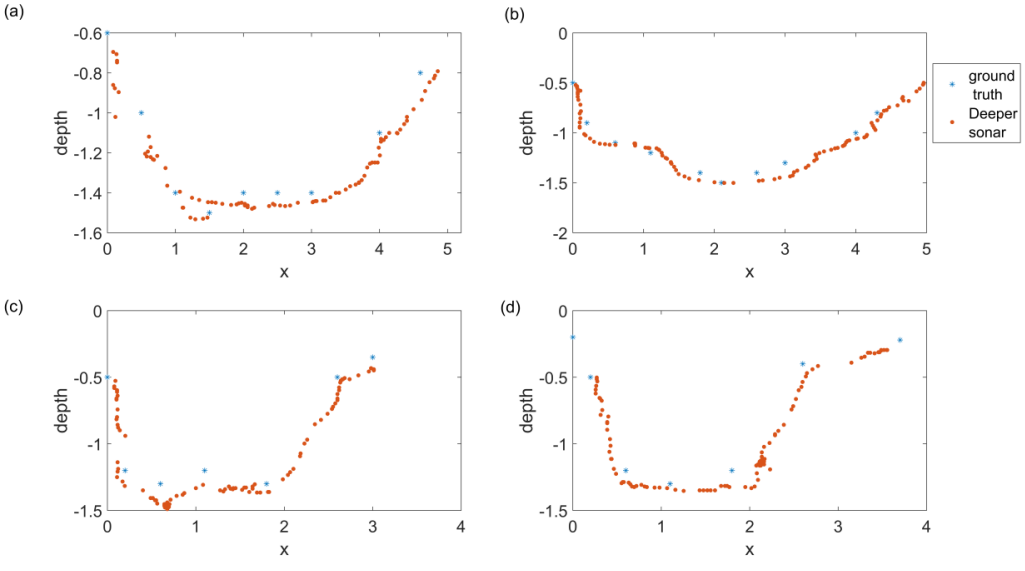

Figure 10. River cross sections retrieved at different locations along Marrebæk Kanal. Red points are retrieved with UAV-borne observations, blue asterisk are the ground truth observations. The latitude and longitude coordinates of the center of the river cross sections are (a) 54.676300°, 11.913296° (b) 54.675507°, 11.913628° (c) 54.682117°, 11.911957° (d) 54.681779°, 11.910723° (WGS84 coordinates).

The accuracy of ground truth observations depends on both i) the accuracy of the GNSS observations ii) the accuracy in positioning the GNSS pole in contact with the river bed. A vertical accuracy of ca. 5-7 cm and a horizontal accuracy of ca. 2-3 cm are estimated for the RTK GNSS ground truth observations. While the accuracy of the UAV-borne river cross section observations depends on i) the error in absolute position of the sonar ii) the sonar's accuracy in measuring depth. The sonar is showing a systematic overestimation of water depth in Figure 10. This confirms that, when high accuracy is required, ground

Hydrol. Earth Syst. Sci. Discuss., https://doi.org/10.5194/hess-2017-625
Manuscript under review for journal Hydrol. Earth Syst. Sci.
Discussion started: 1 November 2017

truth observations are necessary for estimating the bias in sonar measurement. Figure 11 shows the observations after correction for the bias factor, which was ca. 0.95 for this specific survey.

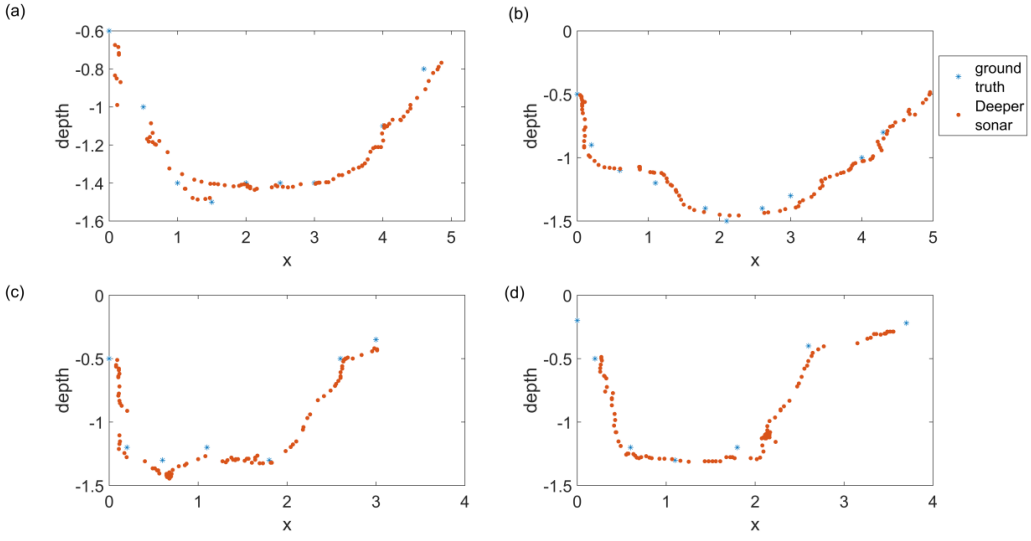

Figure 11. River cross sections observations retrieved from Marrebæk Kanal at the locations shown in Figure 10 after correction of the Deeper sonar observations. Red points are retrieved with UAV-borne observations, blue asterisk are the ground truth observations.

4. Discussion

Bathymetry can be measured with both in situ and remote sensing methods. In-situ methods generally deploy bathymetric sonars installed on vessels. Remote sensing methods include LIDAR techniques, methods evaluating the relationship between spectral signature and depth, or through-water photogrammetry. Remote sensing methods generally allow for larger spatial coverage than in situ methods, but only shallow and clear water bodies can be surveyed. Table 4 shows a comparison of the different remote sensing and in-situ techniques. UAV-borne sonar depth measurements allow to bridge the gap between ground surveys and remote sensing techniques. The tethered sonar can measure deep and turbid water and reach remote and dangerous areas, including non-navigable streams. For depths up to ca. 30 m, the 2.1% accuracy complies with the 1st accuracy level established by the International Hydrographic Organization (IHO) for accurate bathymetric surveys. Indeed, for depths of 30 m, our accuracy results is of ca. 0.630 m, while the 1st IHO level standard requires an accuracy better than 0.634 m. Conversely, for depths greater than 30 m, the UAV-borne sonar measurements comply with the 2nd IHO level.

Hydrol. Earth Syst. Sci. Discuss., https://doi.org/10.5194/hess-2017-625
Manuscript under review for journal Hydrol. Earth Syst. Sci.
Discussion started: 1 November 2017

Hydrology and Earth System Sciences
Discussions

Table 4. Comparison of different approaches for measuring river bathymetry.

Technique	Platform	Spatial resolution (m)	Max. water depth (m)	Typical error (m)	Applicability (e.g. water clarity)	References
Spectral signature	Satellite	High resolution commercial satellites[a]: ≈2 m Medium resolution satellites[b]: Typically›30 m	1-1.5	0.10-0.20	≈1-1.5 times Secchi Depth	(Fonstad and Marcus, 2005; Legleiter and Overstreet, 2012)
	Manned aircraft	Typically 0.5-4				(Carbonneau et al., 2006; Legleiter and Roberts, 2005; Winterbottom and Gilvear, 1997)
	UAV	0.05-0.20				(Flener et al., 2013; Lejot et al., 2007)
Through-water photogrammetry	Manned aircraft	Typically 0.1-0.5	0.6-1.5	0.08-0.2	≈Secchi Depth	(Feurer et al., 2008; Lane et al., 2010; Westaway et al., 2001)
	UAV	Typically 0.01-0.1				(Bagheri et al., 2015; Dietrich, 2016; Tamminga et al., 2014; Woodget et al., 2015)
LIDAR	UAV	≈0.020 m @ 20 m	1-1.5	≈0.10 with standard deviation of 0.13	≈1-1.5 times Secchi Depth	(Mandlburger et al., 2016)
	Manned aircraft	Few dm-several m	6	0.05-0.3	≈2-3 times Secchi Depth	(Bailly et al., 2012, 2010; Charlton et al., 2003; Hilldale and Raff, 2008; Kinzel et al., 2007)
TLS[d]	Banks of the water body	Typically ≈0.05	0.5, but typically ≈0.1	0.005-0.1	Clear water	(Bangen et al., 2014; Heritage and Hetherington, 2007; Smith et al., 2012; Smith and Vericat, 2014)
Single or multi-beam sonars, ADCP[e]	Manned/ Unmanned vessels	Depending on the instrumentation and water depth	Sonars have minimum depth requirements (0.5-1 m)	Variable	Navigable streams	Widely known methodology
Sonar tethered to UAV	UAV	Depending on the water depth[c]	0.5-80	≈3.8%[f] ≈2.1%[g] of actual depth	All water conditions	Methodology described in this paper

[a] Multispectral bands: IKONOS, QuickBird, WorldWiew-2

[b] Landsat

[c] The divergence of the sonar cone beam is 15°.

[d] Terrestrial Laser Scanner (TLS)

[e] Acoustic Doppler Current Profilers (ADCPs)

[f] Before bias correction

[g] After bias correction

Table 4 does not include methods requiring the operator to wade into a river, e.g. measurements taken with a RTK GNSS rover station (e.g. Bangen et al. 2014). To take measurements with a GNSS rover station, the operator must submerge the antenna pole until it reaches the river bed surface. Therefore, this method can only be used for local evaluation of observations, because it cannot retrieve spatially distributed water depth measurements. Furthermore, innovative approaches such as using a ground penetrating radar (GPR) are not included because they are still local proof-of-concept applications (Costa et al., 2000; Spicer et al., 1997) and generally require cableways to suspend instrumentation above river cross sectional area.

In order to obtain reliable measurements and ensure effective post-processing of the data, the techniques shown in Table 4 require initial expenditure and expertise from multiple fields, e.g. electric and software engineers (for technology development and data analysis), pilots (e.g. UAVs and manned aircrafts), experts in river navigations (for boats), surveyors (e.g. for rover GNSS stations, photogrammetry), hydrologists and geologists. In appendix B the typical survey expenditures for the different techniques are shown.

4.1. Future research

UAV-borne measurements of water depth have the potential to enrich the realm of hydrological observations. Their advantages compared to airborne, satellite and manned boat measurements have been proven. The competiveness of UAVs in measuring water depth, compared to the capabilities of unmanned aquatic vessels equipped with sonar and RTK GNSS systems, is currently limited to water bodies that do not allow navigation of unmanned aquatic vessels, e.g. because of high water current, slopes, or obstacles. The full potential of UAV-borne hydrological observations will be exploited only with flight operations beyond visual line-of-sight. The new-generation of waterproof rotary wing UAVs will allow retrieving hyper-spatial observations in remote or dangerous locations, without requiring the operator to access the area.

5. Conclusions

UAVs are flexible and low-cost platforms. They allow operators to retrieve hyper-spatial hydrological observations with high spatial and temporal resolution. Automatic flight, together with computer vision navigation, allows UAVs to monitor dangerous or remote areas, including non-navigable streams.

This study shows how water depths can be retrieved by a tethered sonar controlled by UAVs. In particular we highlight that:

- The sonar accuracy in measuring water depth is not affected by bottom structure and water turbidity if the sound waveform is correctly processed.
- Observations were retrieved for water depths ranging from 0.5 m up to 35 m. Accuracy can be improved from ca. 3.8% to ca. 2.1% after correction of the observational bias, which can be identified and quantified by acquiring a representative sample of ground truth observations. The observational bias is caused by the sound wave's dependence on temperature, salinity and pressure.
- The accuracy and maximum depth capability achieved in this study exceed those of any other remote sensing techniques and are comparable with bathymetric sonars transported by manned or unmanned aquatic vessels.

Hydrol. Earth Syst. Sci. Discuss., https://doi.org/10.5194/hess-2017-625
Manuscript under review for journal Hydrol. Earth Syst. Sci.
Discussion started: 1 November 2017

Hydrology and Earth System Sciences
Discussions
Open Access
EGU

Appendix A

In Figure 8 the measurements of the two different sonars lie along a line with a nearly constant slope (not coincident with the 1:1 line) with respect to the ground truth observations.

Chen and Millero (1977) equation is the international standard algorithm, often known as the UNESCO algorithm, that computes the speed of sound (c) in water as a complex function of temperature (T), salinity (S) and pressure (P) .

This equation has a range of validity: temperature 0 to 40 °C, salinity 0 to 40 parts per thousand, pressure 0 to 1000 bar (Wong and Zhu, 1995). The lake in which the measurements were conducted has a salinity of less than 0.5‰, a recorded surface temperature between 12 and 19°, a depth up to ca. 35 m. After converted from depth to pressure, the equation can be applying to conduct a sensitivity analysis that shows the range of variability of the sound speed with one factor varying at a time, as shown in Figure A1.

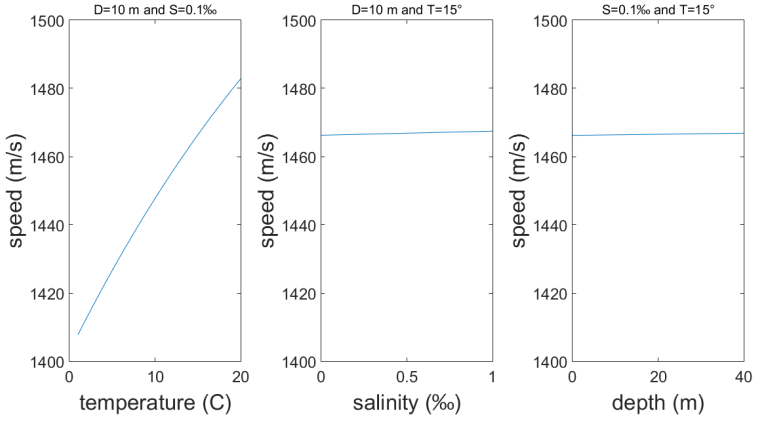

Figure A1. Sound speed for varying temperature, salinity and depth.

As shown Figure A1, temperature has the largest influence on speed of sound. Thus, the slope of linear regression between sonar and ground truth measurements is mainly determined by the temperature profiles and only to a lesser extent by the salinity and depth. Although the two sonars measure the surface temperature of water, no compensation is performed for the temperature vertical profile.

Appendix B

Costs related to the individual approaches to measure bathymetry are hard to estimate and difficult to compare. Costs include an initial expenditure and additional expenses depending on the nature of each survey. These typically depend on the duration of the survey, on the size of the area to be surveyed, on the needed accuracy and resolution, on the cost of labor, and on the water body characteristics. Table B1 compares the approximate costs for the techniques that are most commonly used to retrieve water depth.

Hydrol. Earth Syst. Sci. Discuss., https://doi.org/10.5194/hess-2017-625
Manuscript under review for journal Hydrol. Earth Syst. Sci.
Discussion started: 1 November 2017

Hydrology and Earth System Sciences
Discussions

Table B1. Cost comparison for different techniques.

Technique	Platform	Cost for instrumentation	Costs per survey	Reference
Spectral signature	Satellite	Costs sustained by space agencies	• High resolution: $10-30 per km^2 With minimum order image size: 25-100 km^2 • Medium resolution (e.g. Landsat): open access	http://www.landinfo.com/satellite-imagery-pricing.html
	Manned aircraft	Multispectral Cameras: 15,000-200,000	Minimum survey cost: ~$15,000 to $20,000 Rate per km: $300 to $800 per km^2	Online data collection
	UAV	Multispectral Cameras: 15'000-200'000 Medium size UAV: 3'000-30'000	Minimum survey cost: ~$100-300 per h of survey	Online data collection
Through-water photogrammetry	Manned aircraft	Cameras 5'000-30'000	Minimum survey cost: ~$15,000 to $20,000 Rate per km: $300 to $800 per km^2	Online data collection
	UAV	Cameras 700-10'000 Medium size UAV: 3'000-30'000	Minimum survey cost: ~$100-300 per h of survey	Online data collection
LIDAR	UAV	LIDAR ≈$120'000 Large size UAV: $15'000-30'000	Minimum survey cost: ~$100-300 per h of survey	("Riegl, personal sale quotation" 2017)
	Manned aircraft	LIDAR $100,000-2,500,000 (price range available on the market)	Minimum survey cost: ~$15,000 to $20,000 Rate per km: $300 to $800 per km^2 Post-processing: additional $150 to $300 per km^2	(Bangen et al., 2014)
TLS	In-situ	TLS $65,000–$225,000	Minimum survey cost: ~$60-100 per h Survey efficiency: 1.4–1.9 h/scan	(Bangen et al., 2014)
Single-beam and multi-beam sonar	Manned Boat	• $200-2,000 (single-beam sonar) • $20,000-100,000 (multi-beam sonar)	Minimum survey cost: ~$100-500 per h of survey	Online data collection
Sonar tethered to UAV	UAV	Instrumentation cost: • Sonar $240 • Radar, camera, IMU and GNSS $6000-10000 • Medium size UAV 3'000-30'000	Minimum survey cost: ~$100-300 per h of survey. Survey efficiency: average flight speed of ca. 0.5 m/s	This paper

Acknowledgements

Ole Smith and Mikkel Lund Schmedes from Orbicon A/S provided help and technical support during the on boat bathymetry survey of Furesø.

Funding

The Innovation Fund Denmark is acknowledged for providing funding for this study via the project Smart UAV [125-2013-5].

Alsdorf, D. E., Rodriguez, E. and Lettenmaier, D. P.: Measuring surface water from space, Rev. Geophys., 45, 1–24, doi:10.1029/2006RG000197.1, 2007.

Amir, M. S. I. I., Khan, M. M. ., Rasul, M. G., Sharma, R. H. and Akram, F.: Watershed Delineation and Cross-section Extraction from DEM for Flood Modelling, 19 th Australas. Fluid Mech. Conf., (December), 8–11, 2014.

Bagheri, O., Ghodsian, M. and Saadatseresht, M.: Reach scale application of UAV+SfM method in shallow rivers hyperspatial bathymetry, in International Archives of the Photogrammetry, Remote Sensing and Spatial Information Sciences - ISPRS Archives, vol. 40, pp. 77–81., 2015.

Bailly, J.-S., Kinzel, P. J., Allouis, T., Feurer, D. and Le Coarer, Y.: Airborne LiDAR Methods Applied to Riverine Environments, in Fluvial Remote Sensing for Science and Management, pp. 141–161., 2012.

Bailly, J. S., le Coarer, Y., Languille, P., Stigermark, C. J. and Allouis, T.: Geostatistical estimations of bathymetric LiDAR errors on rivers, Earth Surf. Process. Landforms, 35(10), 1199–1210, doi:10.1002/esp.1991, 2010.

Bandini, F., Jakobsen, J., Olesen, D., Reyna-Gutierrez, J. A. and Bauer-Gottwein, P.: Measuring water level in rivers and lakes from lightweight Unmanned Aerial Vehicles, J. Hydrol., 548, 237–250, doi:10.1016/j.jhydrol.2017.02.038, 2017.

Bangen, S. G., Wheaton, J. M., Bouwes, N., Bouwes, B. and Jordan, C.: A methodological intercomparison of topographic survey techniques for characterizing wadeable streams and rivers, Geomorphology, 206, 343–361, doi:10.1016/j.geomorph.2013.10.010, 2014.

Brown, C. J. and Blondel, P.: Developments in the application of multibeam sonar backscatter for seafloor habitat mapping, Appl. Acoust., 70(10), 1242–1247, doi:10.1016/j.apacoust.2008.08.004, 2009.

Brown, D. C.: Close-range camera calibration, Photogramm. Eng., 37(8), 855–866, doi:10.1.1.14.6358, 1971.

Brown, H. C., Jenkins, L. K., Meadows, G. A. and Shuchman, R. A.: BathyBoat: An autonomous surface vessel for stand-

alone survey and underwater vehicle network supervision, Mar. Technol. Soc. J., 44(4), 20–29, 2010.

Carbonneau, P. E., Lane, S. N. and Bergeron, N.: Feature based image processing methods applied to bathymetric measurements from airborne remote sensing in fluvial environments, Earth Surf. Process. Landforms, 31(11), 1413–1423, doi:10.1002/esp.1341, 2006.

Charlton, M. E., Large, A. R. G. and Fuller, I. C.: Application of airborne lidar in river environments: The River Coquet, Northumberland, UK, Earth Surf. Process. Landforms, 28(3), 299–306, doi:10.1002/esp.482, 2003.

Chen, C. and Millero, F. J.: Speed of sound in seawater at high pressures, J. Acoust. Soc. Am., 62(5), 1129–1135, doi:10.1121/1.381646, 1977.

Clarke, T. and Fryer, J.: The development of camera calibration methods and models, Photogramm. Rec., 16(91), 51–66, doi:10.1111/0031-868X.00113, 1998.

Conner, J. T. and Tonina, D.: Effect of cross-section interpolated bathymetry on 2D hydrodynamic model results in a large river, Earth Surf. Process. Landforms, 39(4), 463–475, doi:10.1002/esp.3458, 2014.

Costa, J. E., Spicer, K. R., Cheng, R. T., Haeni, F. P., Melcher, N. B., Thurman, E. M., Plant, W. J. and Keller, W. C.: Measuring stream discharge by non-contact methods: A proof-of-concept experiment, Geophys. Res. Lett., 27(4), 553–556, doi:10.1029/1999GL006087, 2000.

Detert, M. and Weitbrecht, V.: A low-cost airborne velocimetry system: proof of concept, J. Hydraul. Res., 53(4), 532–539, doi:10.1080/00221686.2015.1054322, 2015.

Dietrich, J. T.: Bathymetric Structure from Motion: Extracting shallow stream bathymetry from multi-view stereo photogrammetry, Earth Surf. Process. Landforms, 42(2), 355–364, doi:10.1002/esp.4060, 2016.

Faig, W.: Calibration of close-range photogrammetry systems: Mathematical formulation, Photogramm Eng Rem S, 41(12), 1479–1486, 1975.

Ferreira, H., Almeida, C., Martins, A., Almeida, J., Dias, N., Dias, A. and Silva, E.: Autonomous bathymetry for risk assessment with ROAZ robotic surface vehicle, in OCEANS '09 IEEE, Bremen: Balancing Technology with Future Needs., 2009.

Feurer, D., Bailly, J.-S., Puech, C., Le Coarer, Y. and Viau, A. A.: Very-high-resolution mapping of river-immersed topography by remote sensing, Prog. Phys. Geogr., 32(4), 403–419, doi:10.1177/0309133308096030, 2008.

Flener, C., Vaaja, M., Jaakkola, A., Krooks, A., Kaartinen, H., Kukko, A., Kasvi, E., Hyyppä, H., Hyyppä, J. and Alho, P.: Seamless mapping of river channels at high resolution using mobile liDAR and UAV-photography, Remote Sens., 5(12), 6382–6407, doi:10.3390/rs5126382, 2013.

Fonstad, M. A. and Marcus, W. A.: Remote sensing of stream depths with hydraulically assisted bathymetry (HAB) models, Geomorphology, 72(1–4), 320–339, doi:10.1016/j.geomorph.2005.06.005, 2005.

Gichamo, T. Z., Popescu, I., Jonoski, A. and Solomatine, D.: River cross-section extraction from the ASTER global DEM for flood modeling, Environ. Model. Softw., 31, 37–46, doi:10.1016/j.envsoft.2011.12.003, 2012.

Giordano, F., Mattei, G., Parente, C., Peluso, F. and Santamaria, R.: Integrating sensors into a marine drone for bathymetric 3D surveys in shallow waters, Sensors, 16(1), doi:10.3390/s16010041, 2015.

Guenther, G. C.: Airborne Lidar Bathymetry, in Digital Elevation Model Technologies and Applications. The DEM Users Manual, p. 253-320 , 8401 Arlington Blvd., 2001.

Guenther, G. C., Cunningham, a G., Larocque, P. E., Reid, D. J., Service, N. O., Highway, E. and Spring, S.: Meeting the Accuracy Challenge in Airborne Lidar Bathymetry, EARSeL eProceedings, 1(1), 1–27, 2000.

Hamylton, S., Hedley, J. and Beaman, R.: Derivation of High-Resolution Bathymetry from Multispectral Satellite Imagery: A Comparison of Empirical and Optimisation Methods through Geographical Error Analysis, Remote Sens., 7(12), 16257–16273, doi:10.3390/rs71215829, 2015.

Heritage, G. L. and Hetherington, D.: Towards a protocol for laser scanning in fluvial geomorphology, Earth Surf. Process. Landforms, 32(1), 66–74, doi:10.1002/esp.1375, 2007.

Hilldale, R. C. and Raff, D.: Assessing the ability of airborne LiDAR to map river bathymetry, Earth Surf. Process. Landforms, 33(5), 773–783, doi:10.1002/esp.1575, 2008.

Kinzel, P. J., Wright, C. W., Nelson, J. M. and Burman, A. R.: Evaluation of an Experimental LiDAR for Surveying a Shallow, Braided, Sand-Bedded River, J. Hydraul. Eng., 133(7), 838–842, doi:10.1061/(ASCE)0733-9429(2007)133:7(838), 2007.

Lane, S. N., Widdison, P. E., Thomas, R. E., Ashworth, P. J., Best, J. L., Lunt, I. A., Sambrook Smith, G. H. and Simpson, C. J.: Quantification of braided river channel change using archival digital image analysis, Earth Surf. Process. Landforms, 35(8), 971–985, doi:10.1002/esp.2015, 2010.

Lee, K. R., Kim, A. M., Olsen;, R. C. and Kruse, F. A.: Using WorldView-2 to determine bottom-type and bathymetry, in Proc. SPIE 8030, Ocean Sensing and Monitoring III, , 80300D (5 May 2011), vol. 2., 2011.

Legleiter, C. J.: Remote measurement of river morphology via fusion of LiDAR topography and spectrally based bathymetry, Earth Surf. Process. Landforms, 37(5), 499–518, doi:10.1002/esp.2262, 2012.

Legleiter, C. J. and Overstreet, B. T.: Mapping gravel bed river bathymetry from space, J. Geophys. Res. Earth Surf., 117(4), doi:10.1029/2012JF002539, 2012.

Legleiter, C. J. and Roberts, D. A.: Effects of channel morphology and sensor spatial resolution on image-derived depth estimates, Remote Sens. Environ., 95(2), 231–247, doi:10.1016/j.rse.2004.12.013, 2005.

Lejot, J., Delacourt, C., Piégay, H., Fournier, T., Trémélo, M.-L. and Allemand, P.: Very high spatial resolution imagery for channel bathymetry and topography from an unmanned mapping controlled platform, Earth Surf. Process. Landforms, 32(11), 1705–1725, doi:10.1002/esp.1595, 2007.

Liceaga-Correa, M. a. and Euan-Avila, J. I.: Assessment of coral reef bathymetric mapping using visible Landsat Thematic Mapper data, Int. J. Remote Sens., 23(1), 3–14, doi:10.1080/01431160010008573, 2002.

Liu, S., Zhang, J. and Ma, Y.: Bathymetric ability of SPOT-5 multi-spectral image in shallow coastal water, in 18th International Conference on Geoinformatics, Geoinformatics 2010., 2010.

Lyons, M., Phinn, S. and Roelfsema, C.: Integrating Quickbird multi-spectral satellite and field data: Mapping bathymetry, seagrass cover, seagrass species and change in Moreton Bay, Australia in 2004 and 2007, Remote Sens., 3(1), 42–64, doi:10.3390/rs3010042, 2011.

Lyzenga, D. R.: Remote sensing of bottom reflectance and water attenuation parameters in shallow water using aircraft and Landsat data, Int. J. Remote Sens., 2(1), 71–82, doi:10.1080/01431168108948342, 1981.

Lyzenga, D. R., Malinas, N. P. and Tanis, F. J.: Multispectral bathymetry using a simple physically based algorithm, IEEE Trans. Geosci. Remote Sens., 44(8), 2251–2259, doi:10.1109/TGRS.2006.872909, 2006.

Mandlburger, G., Pfennigbauer, M., Wieser, M., Riegl, U. and Pfeifer, N.: Evaluation Of A Novel Uav-Borne Topo-Bathymetric Laser Profiler, ISPRS - Int. Arch. Photogramm. Remote Sens. Spat. Inf. Sci., XLI-B1, 933–939, doi:10.5194/isprs-archives-XLI-B1-933-2016, 2016.

Manley, P. L. and Singer, J. K.: Assessment of sedimentation processes determined from side-scan sonar surveys in the Buffalo River, New York, USA, Environ. Geol., 55(7), 1587–1599, doi:10.1007/s00254-007-1109-8, 2008.

Marcus, W. A., Legleiter, C. J., Aspinall, R. J., Boardman, J. W. and Crabtree, R. L.: High spatial resolution hyperspectral mapping of in-stream habitats, depths, and woody debris in mountain streams, Geomorphology, 55(1–4), 363–380, doi:10.1016/S0169-555X(03)00150-8, 2003.

Nitsche, F. O., Ryan, W. B. F., Carbotte, S. M., Bell, R. E., Slagle, A., Bertinado, C., Flood, R., Kenna, T. and McHugh, C.: Regional patterns and local variations of sediment distribution in the Hudson River Estuary, Estuar. Coast. Shelf Sci., 71(1–2), 259–277, doi:10.1016/j.ecss.2006.07.021, 2007.

Powers, J., Brewer, S. K., Long, J. M. and Campbell, T.: Evaluating the use of side-scan sonar for detecting freshwater mussel beds in turbid river environments, Hydrobiologia, 743(1), 127–137, doi:10.1007/s10750-014-2017-z, 2015.

Rovira, A., Batalla, R. J. and Sala, M.: Fluvial sediment budget of a Mediterranean river: The lower Tordera (Catalan Coastal Ranges, NE Spain), Catena, 60(1), 19–42, doi:10.1016/j.catena.2004.11.001, 2005.

Schäppi, B., Perona, P., Schneider, P. and Burlando, P.: Integrating river cross section measurements with digital terrain models for improved flow modelling applications, Comput. Geosci., 36(6), 707–716, doi:10.1016/j.cageo.2009.12.004, 2010.

Smith, M., Vericat, D. and Gibbins, C.: Through-water terrestrial laser scanning of gravel beds at the patch scale, Earth Surf. Process. Landforms, 37(4), 411–421, doi:10.1002/esp.2254, 2012.

Smith, M. W. and Vericat, D.: Evaluating shallow-water bathymetry from through-water terrestrial laser scanning under a range of hydraulic and physical water quality conditions, River Res. Appl., 30(7), 905–924, doi:10.1002/rra.2687, 2014.

Snellen, M., Siemes, K. and Simons, D. G.: Model-based sediment classification using single-beam echosounder signals., J. Acoust. Soc. Am., 129(5), 2878–88, doi:10.1121/1.3569718, 2011.

Spicer, K. R., Costa, J. E. and Placzek, G.: Measuring flood discharge in unstable stream channels using ground-penetrating radar, Geology, 25(5), 423–426, doi:10.1130/0091-7613(1997)025<0423:MFDIUS>2.3.CO, 1997.

Strayer, D. L., Malcom, H. M., Bell, R. E., Carbotte, S. M. and Nitsche, F. O.: Using geophysical information to define benthic

habitats in a large river, Freshw. Biol., 51(1), 25–38, doi:10.1111/j.1365-2427.2005.01472.x, 2006.

Stumpf, R. P., Holderied, K. and Sinclair, M.: Determination of water depth with high-resolution satellite imagery over variable bottom types, Limnol. Oceanogr., 48(1part2), 547–556, doi:10.4319/lo.2003.48.1_part_2.0547, 2003.

Tamminga, a., Hugenholtz, C., Eaton, B. and Lapointe, M.: Hyperspatial Remote Sensing of Channel Reach Morphology and Hydraulic Fish Habitat Using an Unmanned Aerial Vehicle (Uav): a First Assessment in the Context of River Research and Management, River Res. Appl., 31(3), 379–391, doi:10.1002/rra.2743, 2014.

Tauro, F., Petroselli, A. and Arcangeletti, E.: Assessment of drone-based surface flow observations, Hydrol. Process., 30(7), 1114–1130, doi:10.1002/hyp.10698, 2015a.

Tauro, F., Pagano, C., Phamduy, P., Grimaldi, S. and Porfiri, M.: Large-Scale Particle Image Velocimetry From an Unmanned Aerial Vehicle, IEEE/ASME Trans. Mechantronics, 20(6), 1–7, doi:10.1109/TMECH.2015.2408112, 2015b.

Tauro, F., Porfiri, M. and Grimaldi, S.: Surface flow measurements from drones, J. Hydrol., 540, 240–245, doi:10.1016/j.jhydrol.2016.06.012, 2016.

Virili, M., Valigi, P., Ciarfuglia, T. and Pagnottelli, S.: A prototype of radar-drone system for measuring the surface flow velocity at river sites and discharge estimation, Geophys. Res. Abstr., 17(91), 2015–12853, 2015.

Walker, D. J. and Alford, J. B.: Mapping Lake Sturgeon Spawning Habitat in the Upper Tennessee River using Side-Scan Sonar, North Am. J. Fish. Manag., 36(5), 1097–1105, doi:10.1080/02755947.2016.1198289, 2016.

Weng, J., Coher, P. and Herniou, M.: Camera Calibration with Distortion Models and Accuracy Evaluation, IEEE Trans. Pattern Anal. Mach. Intell., 14(10), 965–980, doi:10.1109/34.159901, 1992.

Westaway, R. M., Lane, S. N. and Hicks, D. M.: Remote sensing of clear-water, shallow, gravel-bed rivers using digital photogrammetry, Photogramm. Eng. Remote Sensing, 67(11), 1271–1281, 2001.

Winterbottom, S. J. and Gilvear, D. J.: Quantification of channel bed morphology in gravel-bed rivers using airborne multispectral imagery and aerial photography, Regul. Rivers-Research Manag., 13(6), 489–499, doi:10.1002/(SICI)1099-1646(199711/12)13:6<489::AID-RRR471>3.0.CO;2-X, 1997.

Wong, G. S. K. and Zhu, S.: Speed of sound in seawater as a function of salinity, temperature, and pressure, J. Acoust. Soc. Am., 97(3), 1732–1736, doi:10.1121/1.413048, 1995.

Woodget, A. S., Carbonneau, P. E., Visser, F. and Maddock, I. P.: Quantifying submerged fluvial topography using hyperspatial resolution UAS imagery and structure from motion photogrammetry, Earth Surf. Process. Landforms, 40(1), 47–64, doi:10.1002/esp.3613, 2015.